Long Noncoding RNA MRPL23-AS1 Promotes Adenoid Cystic Carcinoma Lung Metastasis

Chu-Wen Chen[1,2,3,4,5], Min Fu[5], Zhi-Hao Du[5], Fei Zhao[5], Wen-Wen Yang[5], Li-Hua Xu[5], Sheng-Lin Li[1,2,3,4,5], and Xi-Yuan Ge[1,2,3,4,5]

ABSTRACT

Lung metastasis is a major factor affecting long-term survival in patients with adenoid cystic carcinoma. Here, we showed that the long noncoding RNA (lncRNA) MRPL23 antisense RNA 1 (MRPL23-AS1) was highly expressed and correlated with lung metastasis and overall survival in patients with salivary adenoid cystic carcinoma (SACC). MRPL23-AS1 positively regulated epithelial–mesenchymal transition by forming an RNA–protein complex with enhancer of zeste homolog 2 (EZH2). MRPL23-AS1 increased the binding of EZH2 and H3K27me3 on the E-cadherin promoter region. Moreover, MRPL23-AS1 levels were higher in exosomes isolated from the blood plasma of patients with SACC, and exosomal MRPL23-AS1 affected pulmonary microvascular endothelial cells in an "exosomecrine" manner. MRPL23-AS1–enriched exosomes increased microvascular permeability and facilitated the metastasis of SACC *in vivo*. Collectively, these findings highlight a molecular mechanism of lung metastasis in SACC. MRPL23-AS1 may represent a biomarker and target for clinical intervention to control this intractable disease.

Significance: This study identifies a novel metastasis-promoting lncRNA MRPL23-AS1, which mediates the transcriptional silencing of E-cadherin through forming an RNA–protein complex with EZH2.

Introduction

Adenoid cystic carcinoma is a malignant neoplasm that arises within the secretory glands, most commonly in the salivary glands of the head and neck (1). Salivary adenoid cystic carcinoma (SACC), which arises from ductal, myoepithelial, and basal cells, comprises approximately 25% of the malignant tumors in the major salivary glands and approximately 50% of those in the minor glands (2, 3). SACC is a peculiar malignant tumor known for its slow but relentless and infiltrating growth without obvious boundaries. Although SACC tumors are histologically low grade and slow-growing, the distant metastasis rate of SACC can be up to 47.8% (4, 5). Late-onset distant lung metastasis is closely related to the long-term survival rate (6). Surgical dissection and postoperative radiotherapy provide effective local control but do not effectively prevent distant metastasis, and treatment outcomes remain unsatisfactory. In addition, the optimum systemic chemotherapy regimens remain unclear, and there are no approved chemotherapies or targeted agents for the treatment of SACC (1). Therefore, elucidating the biological molecular mechanisms

of SACC lung metastasis is imperative in improving the current situation.

Studies indicate that less than 1.5% of the human genome codes for proteins, and a much larger fraction of the human genome comprises functionally conserved noncoding elements (7). Considerable attention has been focused on long noncoding RNAs (lncRNA), which are a class of transcripts >200 nucleotides (nt) in length with limited protein-coding potential (8). LncRNAs play complex and extensive roles in the development and progression of various cancers (9, 10). Moreover, lncRNAs can be delivered by exosomes and affect tumor cell metastasis through multiple mechanisms (11). Exosomes are 40–150 nm, extracellular, cell-derived phospholipid vesicles of endocytic origin, and they contain functional biomolecules (12–14). Exosomes are secreted by a variety of cells *in vitro* and *in vivo* under physiologic and pathologic conditions, transmitting abundant bioactive molecules to specific recipient cells. Exosomes have been demonstrated to be biomarkers and functional contributors to malignant tumor premetastatic niche formation (13, 15). To date, the specific roles of different exosomal lncRNAs in lung metastasis remain to be clarified.

Our previous research showed that the *EREG*-encoded protein epiregulin, a member of the epidermal growth factor family, promotes SACC lung metastasis via exosomes (16). Epiregulin induces a prometastatic phenotype in SACC cells and increases angiogenesis and the permeability of endothelial cells (16–18). Here, we identified a novel lncRNA, MRPL23 antisense RNA 1 (MRPL23-AS1), which was induced by epiregulin and positively correlated with SACC lung metastasis. MRPL23-AS1 facilitated SACC lung metastasis by recruiting enhancer of zeste homolog 2 (EZH2) and thus negatively regulated the expression of E-cadherin. We also investigated the contribution of exosomal MRPL23-AS1 to the creation of a premetastatic microenvironment in the lungs.

[1]Central Laboratory, Peking University School and Hospital of Stomatology, Beijing, PR China. [2]National Clinical Research Center for Oral Diseases, Beijing, PR China. [3]National Engineering Laboratory for Digital and Material Technology of Stomatology, Beijing, PR China. [4]Beijing Key Laboratory of Digital Stomatology, Beijing, PR China. [5]Department of Oral and Maxillofacial Surgery, Peking University School and Hospital of Stomatology, Beijing, PR China.

Note: Supplementary data for this article are available at Cancer Research Online (http://cancerres.aacrjournals.org/).

C.-W. Chen and M. Fu contributed equally as the co-first authors of this article.

Corresponding Authors: Xi-Yuan Ge and Sheng-Lin Li, Peking University School and Hospital of Stomatology, 22 Zhongguancun South Avenue, Haidian District, Beijing 100081, PR China. Phone: 8610-8219-5537; Fax: 8610-6217-9977; E-mail: gexiyuan@bjmu.edu.cn; and kqshlli@bjmu.edu.cn

Material and Methods

Tissue samples and cell lines

Samples of SACC tissue (205) and submandibular gland (SMG) tissue (56) were obtained from patients who received radical tumor

resection at Peking University Hospital of Stomatology (Beijing, PR China). The patients had received no chemo- or radiotherapy before surgery. The pathologic type of each SACC sample was explicitly diagnosed by histopathologic examination. The patients who were followed for more than five years were selected for the cumulative survival time analysis. The SACC-83 cell line originates from a patient's sublingual gland; SACC-LM cells with enhanced lung metastatic behavior were isolated *in vivo* following the intravenous injection of SACC-83 cells into immunodeficient mice via the tail vein. SACC-83 and SACC-LM cell lines were confirmed by short-tandem repeat PCR analysis, tested *Mycoplasma*-negative by PCR after last experiment, and used within 15 cell passages after thawing. The lentiviral vectors pHBLV-CMV-GFP-T2A-LUC (used to construct the *EREG* expression vector), PHBLV-h-MRPL23-AS1-GFP-LUC (used to construct the MRPL23-AS1 expression vector), and HBLV-h-CDH1-3*flag-RFP-PURO (used to construct the E-cadherin expression vector) were purchased from HanBio (HanBio Biotechnology). After screening, SACC-83 cells stably overexpressing MRPL23-AS1 (MRPL23-AS1 cells) and control cells (Vector cells) were established. Human pulmonary microvascular endothelial cells (HPMEC) were obtained from PriCells and grown in endothelial cell medium (ECM, ScienCell). SACC-83, SACC-LM, Vector (*EREG*-OE Vector), *EREG*-OE, Vector (MRPL23-AS1 Vector), and MRPL23-AS1 cells were maintained in RPMI1640 medium (Gibco) supplemented with 10% FBS (Gibco) and incubated at 37°C in a humidified 5% CO_2 incubator.

Rapid amplification of cDNA ends

tRNA was isolated with TRIzol reagent (Invitrogen). Rapid amplification of cDNA ends (RACE) experiments were performed using the SMARTer RACE 5′/3′ Kit (Clontech) according to the manufacturer's instructions. The sequences of all primers used in this study are shown in Supplementary Table S1.

Overexpression and siRNAs

EREG-OE and SACC-LM cells were transiently transfected with siRNA (si) or scrambled siRNA negative control (si-control). All individual siRNAs were designed and synthesized by RiboBio. The cells were grown in six-well plates to 30%–50% confluence and transfected using riboFECT™ CP (RiboBio) according to the manufacturer's instructions. The cells were harvested after a 48-hour transfection. To overexpress MRPL23-AS1, the plasmid pcDNA-MRPL23-AS1 was constructed by introducing an EcoRI/NotI fragment containing an MRPL23-AS1 cDNA sequence into the same sites in pcDNA3.1(+). MRPL23-AS1 or pcDNA3.1(+) was transfected into SACC-83 cells using Lipofectamine 2000 (Invitrogen).

Microarray expression profiling and gene ontology analysis

Vector and *EREG*-OE cells were subjected to a lncRNA microarray (Agilent Human lncRNA 4 × 180K chip). SACC-LM cells treated with si-control or si-MRPL23-AS1 and SACC-83 cells treated with the control vector or MRPL23-AS1–overexpressing vector were subjected to an mRNA Microarray (Agilent SurePrint G3 Human Gene Expression Microarray 8 × 60K; both by Shbio). Gene ontology (GO) analysis was used to identify the significant biological functions of differentially expressed mRNAs. Specifically, we used a two-sided Fisher exact test to classify the GO terms, and the FDR was calculated to correct the *P* value. The criteria chosen were the number of genes that differed on a certain term/GO ≥ 2, FDR < 0.05, and a *P* value < 0.05.

RNA preparation and qPCR

tRNA was extracted using TRIzol reagent (Invitrogen) according to the manufacturer's instructions, and the extracted RNA was reverse transcribed into cDNA using the cDNA Reverse Transcription Kit (Takara). qPCR was conducted with FastStart Universal SYBR Green Master (ROX) Reagent (Roche) as described on the ABI Prism 7500 Real-Time PCR System (Applied Biosystems). GAPDH was used for normalization. The $2^{-\Delta\Delta C_t}$ method was used to quantify the relative gene expression levels. For the recombinant protein stimulation assay, medium containing different densities of recombinant human epiregulin (rhEpiregulin; Sino Biological) was added to cells and incubated for different lengths of time. Then, the cells were harvested for qPCR to measure RNA expression.

Cell invasion and migration assays

For the invasion assay, the upper chamber of an Insert (Millipore or Falcon) was precoated with Matrigel (BD Biosciences). After 48 hours of treatment, cells were harvested and plated (7×10^4 in 200 μL of serum-free RPMI1640) in the upper chamber with a Matrigel-coated membrane containing 8-μm pores. The inserts were then placed into the lower chamber of a 24-well plate containing RPMI1640 with 10% FBS. After 16 hours, any cells remaining in the upper chamber of the insert were removed with a sterile cotton swab. The invading cells on the bottom surface were stained with 1% crystal violet, examined, counted, and imaged using Digital Microscope (Nikon). The migration assay was performed in the same way as the invasion assay without precoating the upper chamber membrane with Matrigel.

Western blot analysis

Western blot assays were performed according to a standard protocol. The following primary antibodies were used: anti–E-cadherin (3195P, CST), anti–N-cadherin (ab76011, Abcam), anti-CD63 (ab134045, Abcam), anti-EZH2 (ab191080, Abcam) and anti–β-actin (TA-09, ZSGB-Bio). Antibody-bound proteins were detected using an enhanced chemiluminescence (ECL) Western blot kit (CWBio). β-actin or GAPDH was used as the loading control.

RNA-protein pulldown assay

Full-length sense-MRPL23-AS1 and antisense-MRPL23-AS1 were transcribed using T7 MEGAscript kits and labeled using the Pierce RNA 3′ End Desthiobiotinylation Kit (Thermo Fisher Scientific) *in vitro*. RNA pulldown assays were performed using the Pierce Magnetic RNA-Protein Pull Down Kit (Thermo Fisher Scientific). Desthiobiotin-labeled RNA (50 pmol/L) was mixed with 50 μL of magnetic beads and then incubated with the protein lysates from SACC-83 or SACC-LM cells for 60 minutes at 4°C with rotation. The beads were washed briefly four times and boiled in SDS buffer, and the RNA-binding proteins were detected by Western blotting.

RNA immunoprecipitation assay and RIP-seq

RNA immunoprecipitation (RIP) was conducted using the Magna Nuclear RIP (Cross-Linked) Nuclear RNA-Binding Protein Immunoprecipitation Kit (Millipore) according to the manufacturer's protocol. Anti-EZH2 antibodies (ab191250, Abcam; 4905, CST) were used for the RIP assay. Subsequent sequencing after RIP was performed and Tophat (v1.4.0) was used to map the RIP-seq raw reads to the human reference genome (hg19/GRCh37; ref. 19).

Chromatin immunoprecipitation

Chromatin immunoprecipitation (ChIP) was performed using the ChIP Assay Kit (Beyotime) according to the manufacturer's protocol.

Briefly, cross-linked chromatin was sonicated into 200-1,000 bp fragments. The chromatin was immunoprecipitated using anti-EZH2 (ab191250, Abcam) and anti-H3K27me3 (9733S, CST) antibodies. Normal human IgG (ab37415, Abcam) was used as an isotype control. The immunoprecipitated chromatin was purified and analyzed by qPCR. The primers used are listed in the Supplementary Table S1.

Chromatin isolation by RNA purification

Chromatin isolation by RNA purification (ChIRP) was performed using the ChIRP Kit (BersinBio) according to the manufacturer's protocol. Briefly, chromatin was cross-linked and then extracted and fragmented by sonication to 100–500 bp fragments. The chromatin containing the lncRNA MRPL23-AS1 that hybridized to the probes were pulled down using streptavidin-conjugated magnetic beads. The immunoprecipitated chromatin was purified and analyzed by qPCR or Western blotting. A scrambled probe was used as a negative control. The probes were synthesized by RiboBio.

RNA-FISH and immunofluorescence

MRPL23-AS1, 18S, and U6 probes were synthesized by RiboBio. Slides of SACC-83 or SACC-LM cells were fixed in 4% paraformaldehyde for 10 minutes and incubated in PBS containing Triton X-100 at 4°C for 5 minutes. After prehybridization at 37°C for 30 minutes, 102.5 μL of hybridization reaction solution (2.5 μL of probes + 100 μL of hybridization reaction) was added to the slides. The slides were hybridized at 37°C overnight. After that, the slides were washed with 4 × saline sodium citrate (SSC) three times and a descending series of SSC once at 47°C. Finally, the slides were stained with DAPI and subjected to fluorescent signal detection. SACC tissue paraffin-embedded sections were digested with protein K at 37°C for 20 minutes after dewaxing and rehydration. The paraffin sections were subjected to FISH according to the protocol used for the cell slides, except for the prehybridization step. Antibodies (ab191080, Abcam; ZF-0511, ZSBG-BIO) were used to detect EZH2 by immunofluorescence, which was performed according to a standard protocol.

Isolation of cytoplasmic and nuclear RNA

Cytoplasmic and nuclear RNA were isolated and purified using the Nuc-Cyto-Mem Preparation Kit (APPLYGEN) and TRIzol reagent (Invitrogen) according to the manufacturers' instructions.

Exosomes isolation and infection

Exosomes isolation from cells supernatants was performed using ultracentrifugation and sucrose cushion (16). Briefly, cell supernatants were subjected to consecutive centrifugation to remove cellular debris and large vesicles. The supernatants were then passed through a Centrifugal Filter (100K, Millipore) to concentrate followed by a 30% sucrose/deuterium oxide (D_2O) cushion. After gradient centrifugation at $10,0000 \times g$ for 70 minutes using an Optima L-90K Ultracentrifuge (Beckman Coulter), the exosome-enriched sucrose/D_2O was then resuspended in PBS, and the retained exosomes were stored at −80°C. The protein contents of the exosomes were determined using a Bradford Protein Assay Kit (Beyotime Biotechnology). For the patient plasma samples, exosomes and exosomal RNA were isolated using the exoRNeasy Serum/Plasma Maxi Kit (Qiagen) according to the manufacturer's instructions. Exosomes were transfected with full-length MRPL23-AS1 nucleic acid or siRNA using Exo-Fect Exosome Transfection Reagent (SBI) according to the manufacturers' instructions.

Transmission electron microscopy and nanoparticle tracking analysis

After elution with buffer XE (obtained from the exoRNeasy Serum/Plasma Maxi Kit), the exosomes were added to 500 μL of PBS and stored at 4°C prior to analysis. After pretreatment, the samples were examined using a JEM-1400 electron microscope (JEOL). The size distribution and particle concentration of the exosomes were determined by nanoparticle tracking analysis (NTA). Briefly, the exosomes were diluted with PBS (1:20) and measured using NanoSight NS300 (Malvern). The results were analyzed by 3.2 Dev Build 3.2.16.

Mouse model of lung metastasis and the metastatic burden

To identify the role of MRPL23-AS1 in SACC lung metastasis *in vivo*, 1×10^6 Vector- or MRPL23-AS1–transfected cells were injected via the tail vein into NOD/SCID mice (4 weeks, n = 12/group). Bioluminescent Imaging (Caliper Life Sciences) was used to measure the lung metastasis of tumor cells after 8 weeks. The mice were then sacrificed, and their lungs were collected for hematoxylin and eosin (H&E) staining. To compare the contributions of different exosomes to lung metastasis, PBS (100 μL) with Vector-exo or MRPL23-AS1-exo (70 μg) was injected daily into the NOD/SCID (4 weeks, n = 13/group) mice via the tail vein for 5 days. On day 6, the mice received an intravenous injection of 1×10^6 Vector cells. After 8 weeks, bioluminescence was detected. Then, the mice were sacrificed, and their lungs were collected for H&E staining. The metastatic burden within the mouse lungs was quantified by ImageJ software.

Vascular permeability assay

The treated endothelial cells were cultured on Transwell Inserts (0.4 μm pore membrane, Millipore). After forming confluent monolayers for 24 hours, the medium in the upper chamber was replaced by complete medium containing 0.12 mg/mL FITC-labeled Dextran (40 kDa, Sigma-Aldrich). After 2 or 3 hours, 50 μL of the medium in the bottom chamber was harvested, and fluorescence was measured at the condition of excitation 490 nm and emission 520 nm.

Flow cytometric analysis

Exosomes were transfected with antisense/sense MRPL23-AS1 nucleic acids and suspended in 100 μL of PBS. NOD/SCID mice were injected intravenously daily for 5 days with 70 μg of exosomes. On day 6, the mice were sacrificed, and the lungs were collected for murine pulmonary vascular endothelial cell sorting and qPCR. Briefly, lung cells were gently dispersed in collagenase (Sigma) with the MACS Dissociator (Miltenyi Biotec). Endothelial cells were isolated using CD146 Microbeads (Miltenyi Biotec) according to the manufacturer's protocol. The antibody for E-cadherin detection was 3199S(CST), and IgG (4340S, CST) was used as the isotype control.

Study approval

The use of clinical samples was approved by the Ethics Committee of Peking University School and Hospital of Stomatology (Beijing, PR China; Permit number: PKUSSIRB-201522040), and written informed consent was obtained from all patients. All animal handling and procedures were approved by the Peking University Institutional Animal Care and Use Committee (Permit Numbers: LA2015099 and LA2017021).

Statistical analyses

The results were analyzed using SPSS Version 21.0 (IBM). Microarray data and comparison of two groups of data were analyzed using the Student t test to compare two variables. All numerical data

represent the mean ± SD from at least three independent experiments, unless otherwise noted. Log-rank tests were used for the Kaplan–Meier analyses. The correlation coefficient between MRPL23-AS1 expression and clinicopathologic features was calculated using χ^2 test. In cases of multigroup testing, one-way ANOVA was used. A two-tailed $P < 0.05$ was considered statistically significant.

Results

Expression of lncRNA MRPL23-AS1 is upregulated in SACC and positively associated with *EREG*

To determine the downstream lncRNA of *EREG*, we established stable *EREG*-overexpressing SACC-83 cells and performed microarray analysis. One hundred forty-three lncRNAs were upregulated, while 110 lncRNAs were downregulated (fold change ≥ 2, $P <$ 0.05). Eight differentially expressed lncRNAs (**Fig. 1A**) were selected to validate the microarray data by qPCR (**Fig. 1B**). When stimulated with recombinant *EREG* protein, MRPL23-AS1 expression increased significantly (**Fig. 1C** and **D**). MRPL23-AS1 has no protein coding ability according to CPC (http://cpc.cbi.pku.edu.cn/) and CPAT (http://lilab.research.bcm.edu/cpat/). The full-length MRPL23-AS1 transcript was 2,010 nt determined by the 5′ and 3′ RACE method (Supplementary Fig. S1). Overexpressing MRPL23-AS1 reversed the *EREG* knockdown–induced reductions in migration and invasion (**Fig. 1E**). The RNA expression levels of MRPL23-AS1 and *EREG* were found to be higher in the 205 SACC samples than the 56 SMG samples. And as expected, *EREG* expression was positively correlated with MRPL23-AS1 expression (**Fig. 1F**). Moreover, the high expression of MRPL23-AS1 was significantly correlated with a more advanced clinical stage and the presence of lung metastases, as shown in Supplementary Table S2 ($P < 0.05$). The expression level and distribution of MRPL23-AS1 in different cell lines is presented according to lncATLAS (http://lncatlas.crg.eu/) data (**Fig. 2A** and **B**). RT-PCR confirmed a significant increase in MRPL23-AS1 expression in SACC cells compared with HeLa, HepG2, and MCF-7 (**Fig. 2C**). Nuclear and cytoplasmic fractionation and FISH showed that MRPL23-AS1 was mainly located in the nucleus (**Fig. 2D–F**). FISH analysis of paraffin-embedded tissue samples also showed that the expression of MRPL23-AS1 was higher in SACC tissues (**Fig. 2G**). Kaplan–Meier survival analysis showed that the high expression of MRPL23-AS1 was significantly associated with poorer prognosis in terms of cumulative survival (**Fig. 2H**).

MRPL23-AS1 promotes SACC cell epithelial–mesenchymal transition and lung metastasis

MRPL23-AS1 significantly promoted cell migration and invasion (**Fig. 3A–C**). Moreover, a fibroblast-like morphology was observed after MRPL23-AS1 was overexpressed in SACC-83 cells (**Fig. 3D**). Two epithelial–mesenchymal transition (EMT) markers E-cadherin and N-cadherin are involved in the process. (**Fig. 3E**). Stable MRPL23-AS1–overexpressing cells exhibited markedly increased metastatic potential in mouse models (**Fig. 3F** and **G**). IHC staining revealed that tumor nodules had lower expression of E-cadherin (# 3195, CST), and higher expression of the mesenchymal marker N-cadherin (# 13116, CST) in the MRPL23-AS1 group, as compared with the null vector group (Supplementary Fig. S2A and S2B).

MRPL23-AS1 contributes to the binding of EZH2 with the E-cadherin promoter region

The StarBase v3.0 (http://starbase.sysu.edu.cn/) software based on 1.5 million RNA–RNA interactions from multidimensional sequenc-ing data, is used to predict the interaction of lncRNA-mRNA. In starBase, we found no predicted interaction between EZH2 mRNA and MRPL23-AS1. This suggests that MRPL23-AS1 does not interact with EZH2 mRNA. Using an RNA pulldown assay followed by SDS-PAGE detection and silver staining (the antisense sequence was used as an NC), an evident band with a molecular weight of approximately 100 kDa was identified (**Fig. 4A**). MRPL23-AS1 (sense) was found to specifically precipitate EZH2, but EZH2 was not precipitated by the NC (antisense; **Fig. 4B**). Using cross-linked EZH2 RIP-seq, MRPL23-AS1 was identified as one of the lncRNAs that bind to EZH2 (**Fig. 4C**). The RIP-seq data have been deposited in the NCBI Sequence Read Archive (BioProject accession PRJNA562941). RIP-qPCR showed that MRPL23-AS1 was significantly enriched with the anti-EZH2 antibody compared with control (**Fig. 4D**). In addition, a serial deletion analysis revealed that the 1-520 nt region in the 5′ terminal end of the MRPL23-AS1 transcript was critical for the interaction with EZH2 (**Fig. 4E**). The ChIP assay verified the binding of EZH2 to the promoter of E-cadherin (**Fig. 4F**). The ChIRP assay showed the interactions among MRPL23-AS1, EZH2, and the E-cadherin promoter region (**Fig. 4G**).

MRPL23-AS1 contributes to the H3k27me3 of the E-cadherin promoter region via EZH2

A ChIP-qPCR assay showed that MRPL23-AS1 contributed to the H3K27me3 and the binding of EZH2 on the E-cadherin promoter region (**Fig. 5A**). The EZH2 mRNA level changes were consistent with the changes in MRPL23-AS1 expression (**Fig. 5B**), but EZH2 did not change at the protein level (**Fig. 5C**). The colocalization of MRPL23-AS1 and EZH2 was observed using confocal microscopy (**Fig. 5D**). In addition, a significantly negative correlation between E-cadherin and MRPL23-AS1 expression was found in SACC tissues (**Fig. 5E**).

MRPL23-AS1 enhances SACC-83 cell EMT via exosomes

MRPL23-AS1 expression was higher in exosomes derived from SACC-LM, *EREG*-OE, and MRPL23-AS1–overexpressing cells (**Fig. 6A**). Transwell assays showed that MRPL23-AS1 exosomes significantly enhanced the migration and invasion of SACC-83 cells and affected the expression of epithelial markers (**Fig. 6B** and **C**). Full-length transcript sequence or a siRNA specific for MRPL23-AS1 were transfected into exosomes; after being stimulated by differently treated exosomes, SACC cells exhibited changed migratory and invasive abilities as well as changed E-cadherin expression (**Fig. 6D–G**). MRPL23-AS1 expression was examined in human plasma exosomes (**Fig. 6H**). Abundant CD63 protein was found in both groups (**Fig. 6I**), and the transmission electron microscopy experiments showed that the exosomes exhibited a cup- or sphere-shaped morphology (**Fig. 6J**). The NTA results showed that the plasma exosomes from patients with SACC were present in higher concentrations at the most abundant particle size than those from healthy people (**Fig. 6K**).

MRPL23-AS1 induces lung endothelial cell permeability and promotes lung metastasis through exosomes *in vivo*

In addition to EMT, many GO terms were related to vascular development, indicating that MRPL23-AS1 may also be involved in the vascular development process (Supplementary Fig. S3A and S3B). The mRNA microarray data have been deposited in the GEO repository (accession number GSE136698). MRPL23-AS1 promoted the expression of VEGFA via E-cadherin in HPMECs (**Fig. 7A** and **B**). The
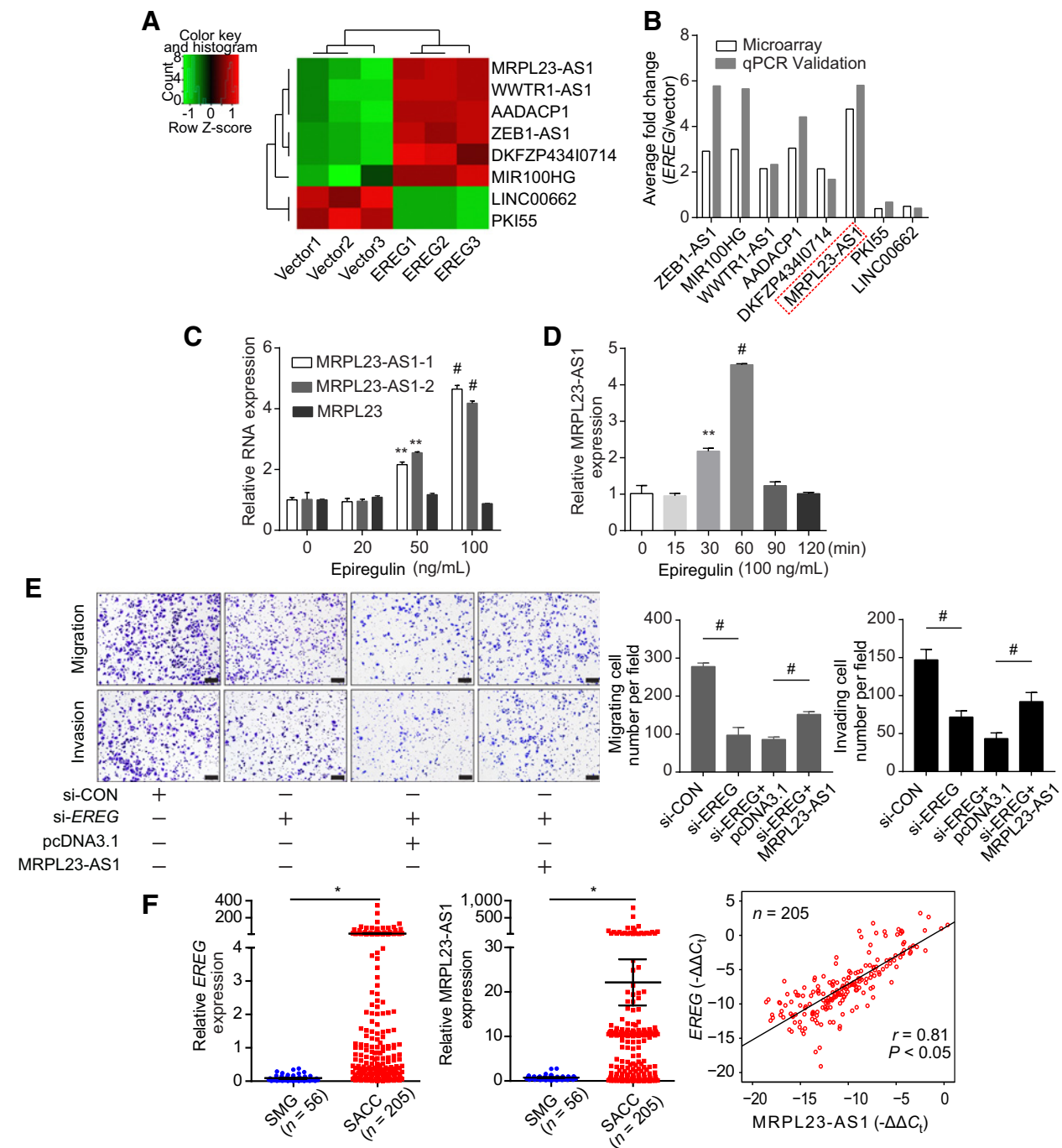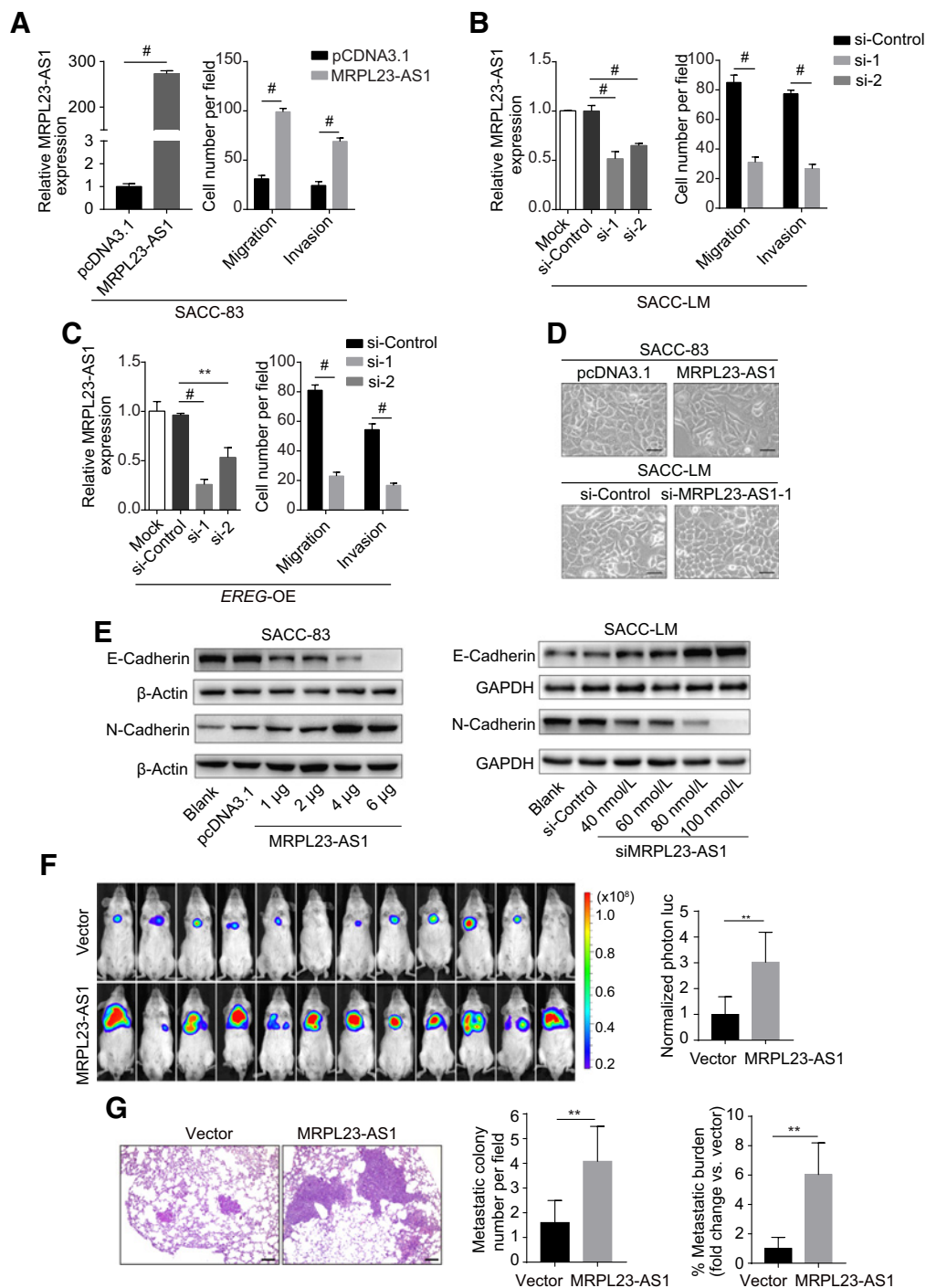
Figure 1.
MRPL23-AS1 is overexpressed in SACC tissue and correlated with *EREG*. **A,** The heatmap and hierarchical clustering of eight selected lncRNAs differentially expressed in *EREG*-OE cells compared with Vector cells are shown. Red, high relative expression; green, low relative expression. **B,** The microarray and qPCR expression data of the selected lncRNAs in the Vector and *EREG*-OE cells are presented. **C** and **D,** For qPCR, GAPDH was used to normalize the C_t values. RT-PCR was used to assess the relative MRPL23-AS1 expression levels using two different pairs of primers in SACC-83 cells after stimulation with epiregulin at different doses (0, 20, 50, and 100 ng/mL; 60 minutes; **C**) or for 0, 15, 30, 60, 90, and 120 minutes (100 ng/mL epiregulin; **D**). **E,** The effect of MRPL23-AS1 overexpression on the *EREG* knockdown–induced migration and invasion of SACC-LM cells. Bar, 100 μm. **F,** RT-PCR was used to analyze the expression of *EREG* (left) and MRPL23-AS1 (middle) in human SACC tissue samples ($n = 205$) and normal SMG tissue samples ($n = 56$). The correlation between *EREG* and MRPL23-AS1 expression in the SACC tissue samples ($n = 205$) is shown (right). Data in **F** (left and middle) are presented as the mean $\pm$ SEM. *, $P < 0.05$; **, $P < 0.01$; #, $P < 0.001$.

Chen et al.
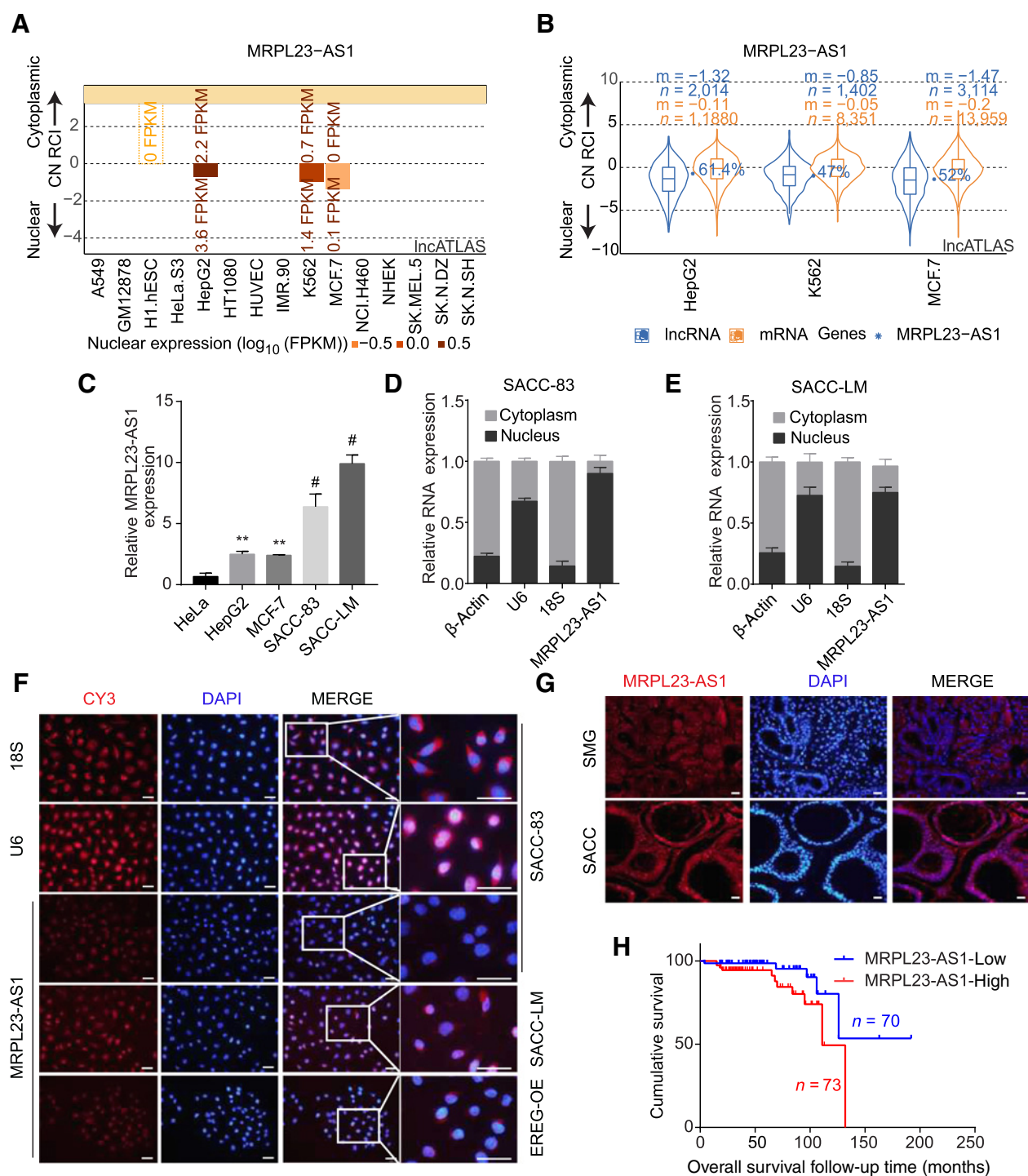
Figure 2.
MRPL23-AS1 is mainly located in the nuclei of SACC cells and is associated with poor prognosis. Cytoplasmic–nuclear localization of MRPL23-AS1 according to the lncATLAS. Relative concentration index (RCI) and expression values (**A**) and RCI distribution (**B**) were recorded. In **B**, "n" indicates the total number of genes in each group, and "m" indicates the median RCI value per group. The group percentile corresponding to each gene is also displayed next to the gene point. **C,** RT-PCR was used to analyze the expression of MRPL23-AS1 in HeLa, HepG2, MCF-7, SACC-83, and SACC-LM cells. **D** and **E,** Nuclear and cytoplasmic fractionation followed by qPCR was used to assess the MRPL23-AS1 expression in SACC-83 and SACC-LM cells. The ratios of the total, nuclear, and cytoplasmic RNA fractions are shown. β-actin, U6, and 18S were used as endogenous controls. **F** and **G,** An RNA-FISH assay was used to determine the intracellular localization of MRPL23-AS1 in SACC-83, SACC-LM, and *EREG*-OE cells. U6 and 18S were used as endogenous controls (**F**). MRPL23-AS1 expression levels were examined in SACC and SMG tissue samples (**G**). MRPL23-AS1 RNA-FISH probe sets were labeled with Cy3 (red), and cell nuclei were labeled with the DNA dye DAPI (blue). Bar, 20 μm. $n = 8$. **H,** Kaplan–Meier curves for cumulative survival time ($n = 143$) are shown. **, $P < 0.01$; #, $P < 0.001$.

Figure 3.
MRPL23-AS1 promotes SACC EMT *in vitro* and lung metastasis *in vivo*. **A,** Expression of MRPL23-AS1 in SACC-83 cells transfected with the control vector (pcDNA3.1) or the MRPL23-AS1 expression vector (MRPL23-AS1; left). Transwell assays of SACC-83 cells transiently transfected with MRPL23-AS1 or the control plasmid (right). **B** and **C,** Expression of MRPL23-AS1 in SACC-LM cells and *EREG*-OE cells transfected with si-MRPL23-AS1 or si-control (**B**, left and **C**, left). Transwell assays of SACC-LM and *EREG*-OE cells transfected with si-MRPL23-AS1 or si-control (**B,** right and **C**, right). **D,** Phase-contrast microscopy of SACC-83 cells transiently overexpressing MRPL23-AS1 (compared with SACC-83 cells transiently expressing pcDNA3.1) and MRPL23-AS1 expression knockdown SACC-LM cells (compared with SACC-LM cells treated with si-control). Scale bar, 50 μm. **E,** Western blot analysis of the E-cadherin and N-cadherin expression levels in SACC-83 and SACC-LM cells. **F,** Left, visualization of the lung metastases that developed after the intravenous injection of Vector or MRPL23-AS1 cells into NOD/SCID mice. Right, representative images of the bioluminescent signals and normalized photon flux. **G,** Representative images (left) and quantification of the metastatic tumor nodules and tumor burden (right) in lung sections from NOD/SCID mice intravenously injected with Vector or MRPL23-AS1 cells ($n = 12$/group). Scale bar, 50 μm. All experiments *in vitro* were performed with at least three biological replicates. **, $P < 0.01$; #, $P < 0.001$.

Chen et al.
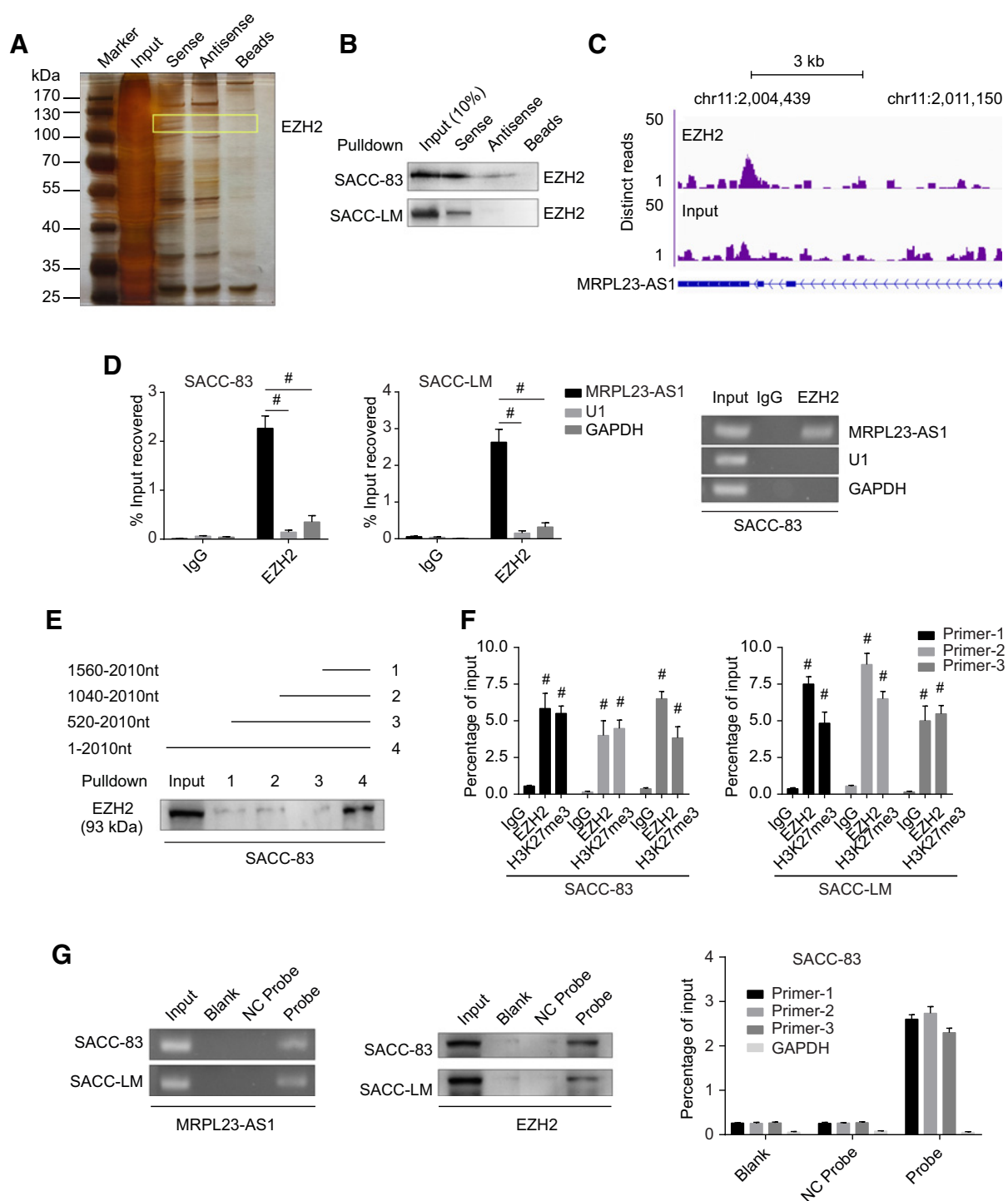
Figure 4.
MRPL23-AS1 contributes to the binding of EZH2 on the E-cadherin promoter region. **A,** A representative silver-stained PAGE gel is shown. Antisense MRPL23-AS1 was used as the nonspecific control. **B,** The specific association of MRPL23-AS1 with the EZH2 protein was validated through RNA pulldown, followed by Western blotting. **C,** The RIP-seq profile shows the pulldown of MRPL23-AS1 by EZH2. Both the RIP-seq and input samples were normalized to the same sequencing depth. **D,** RT-PCR was used to measure the RNA enrichment in the RIP assay using the anti-EZH2 antibody in SACC-83 and SACC-LM cells. Normal IgG was used as the nonspecific control antibody. U1 and GAPDH were used as negative controls. **E,** Serial deletions of MRPL23-AS1 were used in the RNA pulldown assays. **F,** ChIP-qPCR analysis was used to assess the EZH2 genomic occupancy and H3K27 methylation status of the E-cadherin promoter in SACC-83 (left) and SACC-LM (right) cells. **G,** ChIRP-qPCR of MRPL23-AS1 (left) and Western blot analysis of pulled down protein components (middle) from SACC-83 and SACC-LM cells are shown. Three different primer pairs were used to determine the RNA enrichment of the E-cadherin promoter region in SACC-83 cells by ChIRP-qPCR (right). #, $P < 0.001$.

perfusion of MRPL23-AS1–transfected exosomes increased the leakage of Evans blue in mouse lungs (**Fig. 7C**). In addition, E-cadherin expression was significantly decreased in CD146$^+$-sorted lung endothelial cells following stimulation with the sense exosomes (**Fig. 7D**). The MRPL23-AS1–transfected exosomes significantly enhanced the

expression of VEGFA and decreased E-cadherin and VE-cadherin expression in the CD146$^+$-sorted lung endothelial cells (**Fig. 7E** and **F**). Finally, the intravenous injection of exosomes from MRPL23-AS1–overexpressing cells into immunodeficient mice significantly increased SACC lung metastases (**Fig. 7G** and **H**).
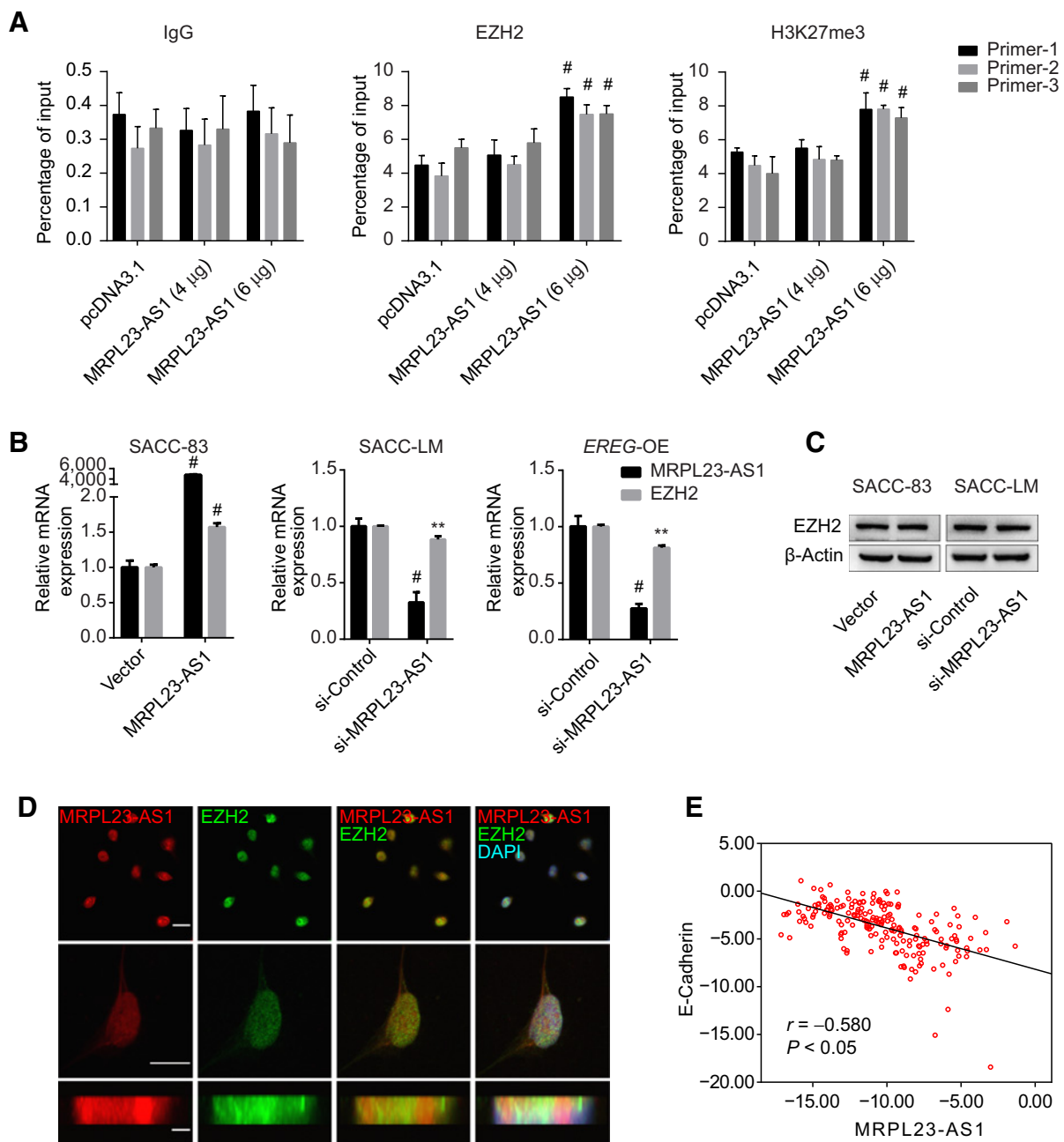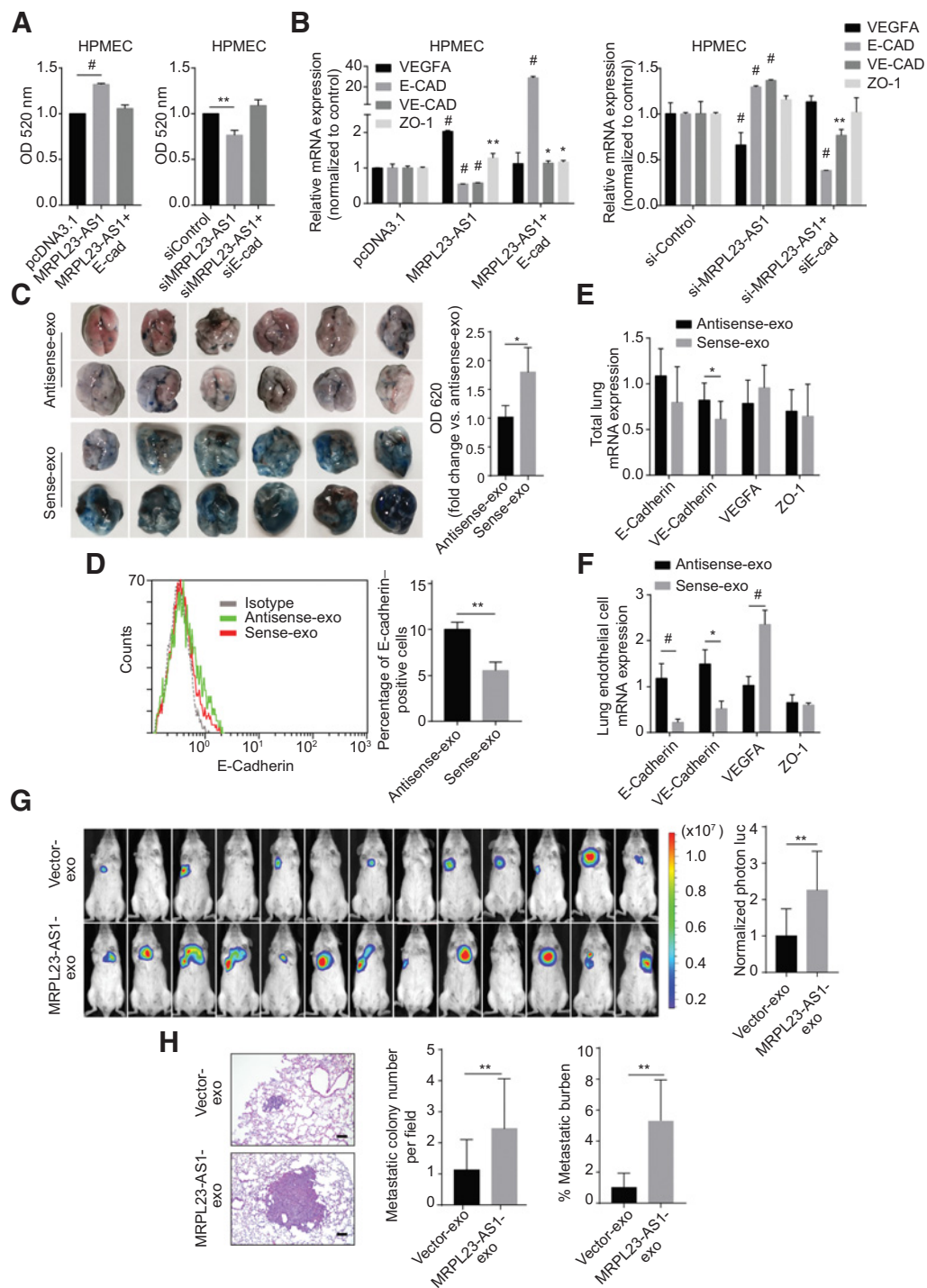

Figure 5.
MRPL23-AS1 promotes methylation of the E-cadherin promoter region by scaffolding EZH2. **A,** ChIP-qPCR analysis was used to assess the EZH2 genomic occupancy and H3K27 methylation status of the E-cadherin promoter in SACC-83 cells with different levels of MRPL23-AS1 overexpression. Three different primers were used to determine the protein enrichment in the E-cadherin promoter region by qPCR. **B** and **C,** RT-PCR and Western blot analysis were used to determine the mRNA (**B**) and protein (**C**) expression of EZH2, respectively, after altering MRPL23-AS1 expression in SACC cells. **D,** The intracellular locations of MRPL23-AS1 and EZH2 in SACC-83 cells were identified using RNA-FISH and immunofluorescence, respectively, followed by confocal microscopy analysis. The MRPL23-AS1 RNA-FISH probe sets were labeled with Cy3 (red), the anti-EZH2 antibody was labeled with Alexa Fluor 488 (green), and the nuclei were labeled with the DNA dye DAPI (blue). Scale bars, 10 μm, 5 μm, and 1 μm (from top to bottom). **E,** The correlation between MRPL23-AS1 and E-cadherin mRNA expression in the SACC tissue samples ($n = 205$) was assessed. **, $P < 0.01$; #, $P < 0.001$.

Chen et al.
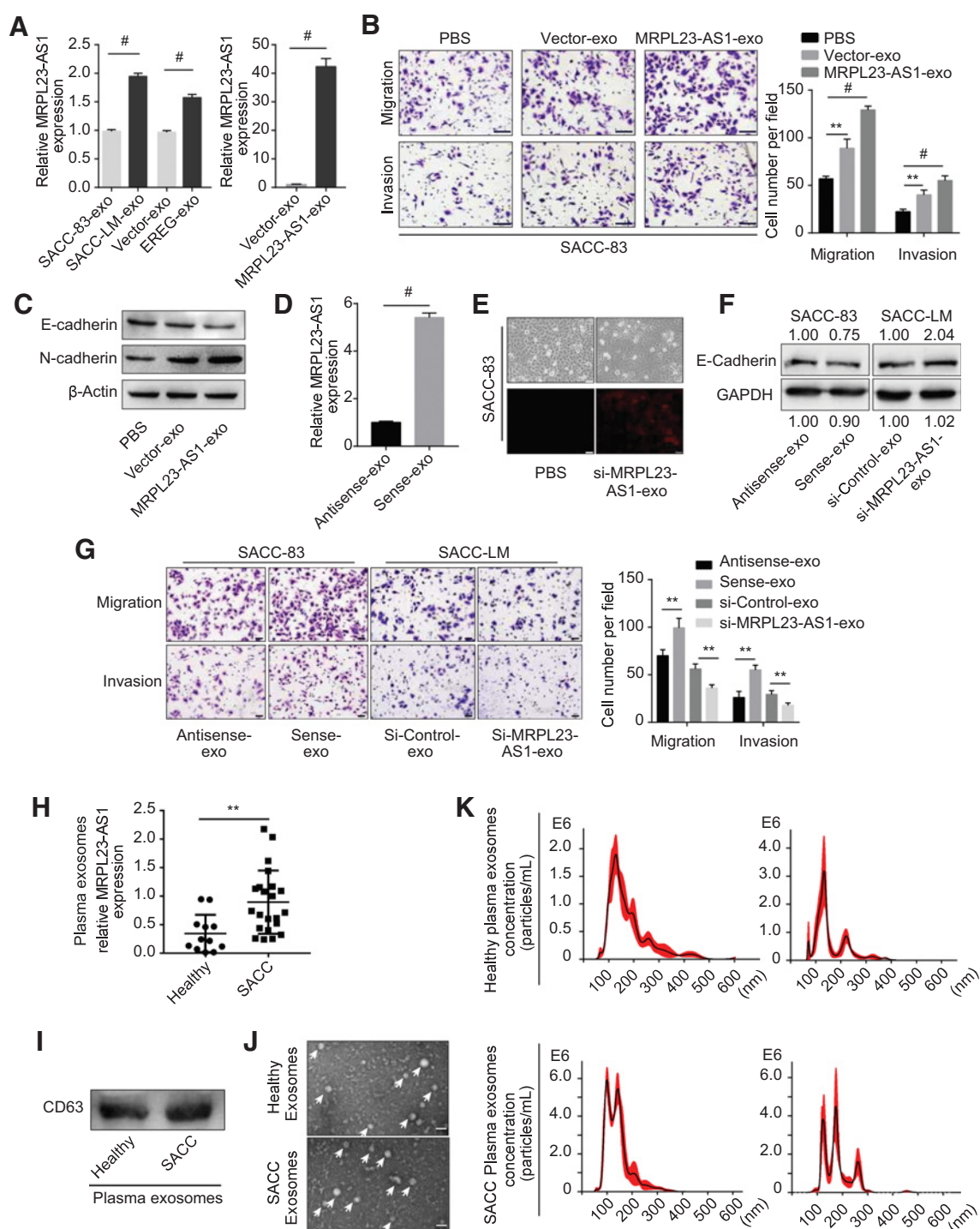
Figure 6.
MRPL23-AS1 induces EMT in SACC cells through exosomes. **A,** The expression levels of MRPL23-AS1 in exosomes derived from different SACC cells were determined by qPCR. **B,** Transwell assays were used to assess SACC-83 cells after an incubation with PBS, Vector-exo, or MRPL23-AS1-exo. **C,** The corresponding epithelial markers (E-cadherin and N-cadherin) were evaluated by Western blotting. Bar, 50 μm. The efficiencies of exosomes transfections were evaluated by qPCR in SACC-83 cells (**D**) and by fluorescence observation in SACC-LM cells. Exosomes were transfected with fluorescently labeled siRNA and then added to the target cells (**E**). Bar, 50 μm. **F,** E-cadherin expression levels were determined by Western blotting after transfection. **G,** Transwell assays were used to assess SACC-83 and SACC-LM cells after incubation with differently treated exosomes. Bar, 50 μm. **H,** Plasma exosomes from healthy people ($n = 12$) and patients with SACC ($n = 22$) were isolated and subjected to RNA extraction and qPCR to determine the MRPL23-AS1 expression levels. **I,** CD63 expression in human plasma exosomes was determined by Western blotting. **J,** Transmission electron microscopy images of human plasma exosomes are shown. Bar, 50 nm. **K,** NTA was used to determine the particle size and concentration of human plasma exosomes. **, $P < 0.01$; #, $P < 0.001$.

Figure 7.
Effects of exosomal MRPL23-AS1 on the permeability of lung endothelial cells and lung metastasis *in vivo*. **A** and **B,** Permeability assays (**A**) and RT-PCR of the relative VEGFA, E-cadherin, VE-cadherin, and ZO-1 mRNA expression levels (**B**) in differently treated HPMEC cells. The results are expressed as the fold change relative to the control group. **C,** Representative images (left) and quantification (right) of Evans blue leakage in the lungs of nude mice 5 days after stimulation with sense or antisense exosomes (*n* = 12/group). **D,** Flow cytometric analysis of E-cadherin expression in CD146^{+}-sorted lung endothelial cells from mice. The relative percentage of positive cells is shown. **E** and **F,** RT-PCR of VEGFA, E-cadherin, VE-cadherin, and ZO-1 mRNA expression in the total lungs (**E**) and in the CD146^{+}-sorted murine endothelial cells (**F**) obtained from treated mice (*n* = 10/group). **G** and **H,** Formation of lung metastases in mice after stimulation with Vector-exo or MRPL23-AS1-exo, as represented by bioluminescence signals (left) and normalized photon flux (right; **G**) or representative images (left) and quantification (right) of the metastatic tumor nodules and metastatic burden in lung sections from NOD/SCID mice (**H**; *n* = 13/group). Bar, 50 μm. All experiments *in vitro* were performed with at least three biological replicates. *, *P* < 0.05; **, *P* < 0.01; #, *P* < 0.001.

Discussion

Despite the therapeutic advances made in SACC, the long-term prognosis of patients with distant metastasis remains unsatisfactory as a result of our limited understanding of the underlying mechanisms of metastasis. In addition, lncRNAs have been identified to be involved in the initiation and progression of cancer, indicating their clinical potential as biomarkers and therapeutic targets (9, 10, 20). Here, we showed that the expression of MRPL23-AS1 was positively associated with *EREG*, a lung metastasis–associated gene (18), in SACC cell lines and tissue samples. Transcription factors could regulate lncRNA expression by direct binding to its promoter region. In our study, the transcription factor E2F1, which has been found to regulate the expression of many lncRNA, such as HOXA11-AS (21), ERIC (22), and ANRIL (23), is upregulated in *EREG*-OE cells, as compared with null Vector cells. The JASPAR database (24) predicted the potential E2F1 binding site within the MRPL23-AS1 promoter region. Therefore, E2F1 might be a regulator involved in *EREG*-mediated upregulation of MRPL23-AS1. Recent studies have shown that many lncRNAs are individually required for the proper localization of specific genomic regulators and lead to the inactivation of tumor suppressors or activation of oncogenes by guiding and recruiting histone protein modification enzymes, or transcription factors (25). We identified E-cadherin as a downstream target gene of MRPL23-AS1, and MRPL23-AS1 could mediate the transcriptional silencing of E-cadherin through EZH2-mediated H3K27me3.

In addition to traditional cell communication methods, such as juxtacrine, paracrine, endocrine, exocrine, or synaptic mechanisms, the discovery of exosome involvement in cell-to-cell communication has provided new insights into cell signaling (26). In our previous study, we proposed the term "exosomecrine" to denote cell-to-cell signaling transduction via the exosome-mediated transfer of molecules (16). The nature of exosome mediation, which enables near or distant cell communication, distinguishes exosomecrine signaling from other cell communication patterns. The spread of tumor-promoting molecules is a crucial function of cancer cell–derived exosomes (26, 27). For example, lncARSR can be incorporated into exosomes and transmitted to disseminate sunitinib resistance to sensitive cells in renal cancer (28); exosomal PD-L1 contributes to immunosuppression and could be developed as a predictor for the clinical outcomes of anti–PD-1 therapy in patients with metastatic melanoma (29). Currently, the contribution of exosomal lncRNAs to lung metastasis remains unclear. MRPL23-AS1–enriched exosomes promoted the migration and invasion of SACC cells. To support a precise causal relationship solely between exosomal MRPL23-AS1 and the changes in recipient cells, we transfected exosomes derived from SACC-83 cells with full-length MRPL23-AS1 and exosomes derived from SACC-LM cells with siRNAs specific for MRPL23-AS1. The MRPL23-AS1–transfected exosomes enhanced EMT, and the si-MRPL23-AS1–transfected exosomes reduced EMT in SACC cells. These observations illustrated the independent role of internalized exosomal MRPL23-AS1 in promoting the migration and invasion of tumor cells in the primary tumor microenvironment.

Cancer-secreted exosomes can also be internalized by other cell types in distant premetastatic or metastatic niches (13, 30, 31). Exosomes can be isolated from the plasma, serum, urine, and pleural and ascetic effusions of patients with cancer (32–34). Recently, plasma exosomal lncRNAs have been proposed as potential early diagnostic and prognostic biomarkers (28, 35). We found that the MRPL23-AS1 content was higher in the patient plasma exosomes than in the

healthy control exosomes. In addition, NTA showed that the particle concentration and size of the plasma exosomes from patients with SACC were higher than those from healthy people, suggesting that the change in plasma exosomes might act on the premetastatic niche and might be associated with the distant metastasis of SACC. Compared with the intravenous injection of control exosomes, intravenous injection of MRPL23-AS1–enriched exosomes significantly increased the number of SACC lung metastases in an immunodeficient mouse model. MRPL23-AS1 promotes the expression of VEGF and inhibits the expression of E-cadherin. Although miR-9–mediated E-cadherin downregulation has been reported to result in the activation of β-catenin signaling, which contributes to the upregulated expression of VEGF (36), there are currently no reports on the E-cadherin–mediated regulation of VEGFA in endothelial cells. Our study showed that MRPL23-AS1 promoted the expression of VEGFA via E-cadherin in HPMECs through an *in vitro* rescue assay. Increasing vascular permeability is believed to be an early event in the metastatic process of malignant tumor cells (37), and exosomal MRPL23-AS1 increased the permeability of mouse pulmonary microvascular endothelial cells. Moreover, MRPL23-AS1–transfected exosomes decreased the expression of E-cadherin and increased the expression of VEGF in CD146$^+$-sorted mouse lung microvascular endothelial cells. This result confirmed the role of exosomecrine communication in distant premetastatic niche formation in the lungs. Several studies have reported that VEGF regulates VE-cadherin and ZO-1 expression through different mechanisms, which results in increased permeability in vascular endothelial cells (38–40).

Collectively, our findings identify a new lncRNA, MRPL23-AS1, that promotes the inactivation of the key metastasis suppressor, E-cadherin, through EZH2-induced promoter hypermethylation. Moreover, MRPL23-AS1 could be delivered via exosomes to act on distant target cells, specifically pulmonary microvascular endothelial cells in the premetastatic niche, increasing microvascular permeability and thus facilitating lung metastasis in SACC.

References

1. Drier Y, Cotton MJ, Williamson KE, Gillespie SM, Ryan RJH, Kluk MJ, et al. An oncogenic MYB feedback loop drives alternate cell fates in adenoid cystic carcinoma. Nat Genet 2016;48:265–72.
2. Renehan A, Gleave EN, Hancock BD, Smith P, McGurk M. Long-term follow-up of over 1000 patients with salivary gland tumours treated in a single centre. Br J Surg 1996;83:1750–4.
3. Anderson JN Jr., Beenken SW, Crowe R, Soong SJ, Peters G, Maddox WA, et al. Prognostic factors in minor salivary gland cancer. Head Neck 1995;17:480–6.
4. Fordice J, Kershaw C, El-Naggar A, Goepfert H. Adenoid cystic carcinoma of the head and neck: predictors of morbidity and mortality. Arch Otolaryngol Head Neck Surg 1999;125:149–52.
5. Rapidis AD, Givalos N, Gakiopoulou H, Faratzis G, Stavrianos SD, Vilos GA, et al. Adenoid cystic carcinoma of the head and neck. clinicopathological analysis of 23 patients and review of the literature. Oral Oncol 2005;41:328–35.
6. Gao M, Hao Y, Huang MX, Ma DQ, Luo HY, Gao Y, et al. Clinicopathological study of distant metastases of salivary adenoid cystic carcinoma. Int J Oral Maxillofac Surg 2013;42:923–8.
7. Lander ES. Initial impact of the sequencing of the human genome. Nature 2011;470:187–97.
8. Mercer TR, Dinger ME, Mattick JS. Long non-coding RNAs: insights into functions. Nat Rev Genet 2009;10:155–9.
9. Kopp F, Mendell JT. Functional classification and experimental dissection of long noncoding RNAs. Cell 2018;172:393–407.
10. Lin C, Yang L. Long noncoding RNA in cancer: wiring signaling circuitry. Trends Cell Biol 2018;28:287–301.
11. Fan Q, Yang L, Zhang X, Peng X, Wei S, Su D, et al. The emerging role of exosome-derived non-coding RNAs in cancer biology. Cancer Lett 2018;414:107–15.
12. Raposo G, Stoorvogel W. Extracellular vesicles: exosomes, microvesicles, and friends. J Cell Biol 2013;200:373–83.
13. Costa-Silva B, Aiello NM, Ocean AJ, Singh S, Zhang H, Thakur BK, et al. Pancreatic cancer exosomes initiate pre-metastatic niche formation in the liver. Nat Cell Biol 2015;17:816–26.
14. Hoshino A, Costa-Silva B, Shen TL, Rodrigues G, Hashimoto A, Tesic Mark M, et al. Tumour exosome integrins determine organotropic metastasis. Nature 2015;527:329–35.
15. Peinado H, Zhang H, Matei IR, Costa-Silva B, Hoshino A, Rodrigues G, et al. Pre-metastatic niches: organ-specific homes for metastases. Nat Rev Cancer 2017;17:302–17.
16. Yang WW, Yang LQ, Zhao F, Chen CW, Xu LH, Fu J, et al. Epiregulin promotes lung metastasis of salivary adenoid cystic carcinoma. Theranostics 2017;7:3700–14.
17. Kaplan RN, Riba RD, Zacharoulis S, Bramley AH, Vincent L, Costa C, et al. VEGFR1-positive haematopoietic bone marrow progenitors initiate the pre-metastatic niche. Nature 2005;438:820–7.
18. Gupta GP, Nguyen DX, Chiang AC, Bos PD, Kim JY, Nadal C, et al. Mediators of vascular remodelling co-opted for sequential steps in lung metastasis. Nature 2007;446:765–70.
19. Trapnell C, Roberts A, Goff L, Pertea G, Kim D, Kelley DR, et al. Differential gene and transcript expression analysis of RNA-seq experiments with TopHat and Cufflinks. Nat Protoc 2012;7:562–78.
20. Evans JR, Feng FY, Chinnaiyan AM. The bright side of dark matter: lncRNAs in cancer. J Clin Invest 2016;126:2775–82.
21. Sun M, Nie F, Wang Y, Zhang Z, Hou J, He D, et al. LncRNA HOXA11-AS promotes proliferation and invasion of gastric cancer by scaffolding the chromatin modification factors PRC2, LSD1, and DNMT1. Cancer Res 2016;76:6299–310.
22. Feldstein O, Nizri T, Doniger T, Jacob J, Rechavi G, Ginsberg D. The long non-coding RNA ERIC is regulated by E2F and modulates the cellular response to DNA damage. Mol Cancer 2013;12:131.
23. Wan G, Mathur R, Hu X, Liu Y, Zhang X, Peng G, et al. Long non-coding RNA ANRIL (CDKN2B-AS) is induced by the ATM-E2F1 signaling pathway. Cell Signal 2013;25:1086–95.
24. Khan A, Fornes O, Stigliani A, Gheorghe M, Castro-Mondragon JA, van der Lee R, et al. JASPAR 2018: update of the open-access database of transcription factor binding profiles and its web framework. Nucleic Acids Res 2018;46:D260–D6.
25. Rinn JL, Chang HY. Genome regulation by long noncoding RNAs. Annu Rev Biochem 2012;81:145–66.
26. Jelonek K, Widlak P, Pietrowska M. The influence of ionizing radiation on exosome composition, secretion and intercellular communication. Protein Pept Lett 2016;23:656–63.
27. Zomer A, Maynard C, Verweij FJ, Kamermans A, Schafer R, Beerling E, et al. In vivo imaging reveals extracellular vesicle-mediated phenocopying of metastatic behavior. Cell 2015;161:1046–57.
28. Qu L, Ding J, Chen C, Wu ZJ, Liu B, Gao Y, et al. Exosome-transmitted lncARSR promotes sunitinib resistance in renal cancer by acting as a competing endogenous RNA. Cancer Cell 2016;29:653–68.
29. Chen G, Huang AC, Zhang W, Zhang G, Wu M, Xu W, et al. Exosomal PD-L1 contributes to immunosuppression and is associated with anti-PD-1 response. Nature 2018;560:382–6.
30. Yan W, Wu XW, Zhou WY, Fong MY, Cao MH, Liu J, et al. Cancer-cell-secreted exosomal miR-105 promotes tumour growth through the MYC-dependent metabolic reprogramming of stromal cells. Nat Cell Biol 2018;20:597–609.
31. Zhou W, Fong MY, Min Y, Somlo G, Liu L, Palomares MR, et al. Cancer-secreted miR-105 destroys vascular endothelial barriers to promote metastasis. Cancer Cell 2014;25:501–15.
32. Melo SA, Luecke LB, Kahlert C, Fernandez AF, Gammon ST, Kaye J, et al. Glypican-1 identifies cancer exosomes and detects early pancreatic cancer. Nature 2015;523:177–82.
33. Xu R, Rai A, Chen M, Suwakulsiri W, Greening DW, Simpson RJ. Extracellular vesicles in cancer - implications for future improvements in cancer care. Nat Rev Clin Oncol 2018;15:617–38.
34. Andre F, Schartz NE, Movassagh M, Flament C, Pautier P, Morice P, et al. Malignant effusions and immunogenic tumour-derived exosomes. Lancet 2002;360:295–305.
35. Ren J, Ding L, Zhang D, Shi G, Xu Q, Shen S, et al. Carcinoma-associated fibroblasts promote the stemness and chemoresistance of colorectal cancer by transferring exosomal lncRNA H19. Theranostics 2018;8:3932–48.
36. Ma L, Young J, Prabhala H, Pan E, Mestdagh P, Muth D, et al. miR-9, a MYC/MYCN-activated microRNA, regulates E-cadherin and cancer metastasis. Nat Cell Biol 2010;12:247–56.
37. Peinado H, Aleckovic M, Lavotshkin S, Matei I, Costa-Silva B, Moreno-Bueno G, et al. Melanoma exosomes educate bone marrow progenitor cells toward a pro-metastatic phenotype through MET. Nat Med 2012;18:883–91.
38. Li X, Padhan N, Sjostrom EO, Roche FP, Testini C, Honkura N, et al. VEGFR2 pY949 signalling regulates adherens junction integrity and metastatic spread. Nat Commun 2016;7:11017.
39. Giannotta M, Trani M, Dejana E. VE-cadherin and endothelial adherens junctions: active guardians of vascular integrity. Dev Cell 2013;26:441–54.
40. Lee SW, Kim WJ, Choi YK, Song HS, Son MJ, Gelman IH, et al. SSeCKS regulates angiogenesis and tight junction formation in blood-brain barrier. Nat Med 2003;9:900–6.

Cancer Research

The Journal of Cancer Research (1916–1930) | The American Journal of Cancer (1931–1940)

AAC R American Association for Cancer Research

Long Noncoding RNA MRPL23-AS1 Promotes Adenoid Cystic Carcinoma Lung Metastasis

Chu-Wen Chen, Min Fu, Zhi-Hao Du, et al.

Updated version	Access the most recent version of this article at: doi:10.1158/0008-5472.CAN-19-0819
Supplementary Material	Access the most recent supplemental material at: http://cancerres.aacrjournals.org/content/suppl/2020/02/25/0008-5472.CAN-19-0819.DC1

Cited articles	This article cites 40 articles, 2 of which you can access for free at: http://cancerres.aacrjournals.org/content/80/11/2273.full#ref-list-1

E-mail alerts	Sign up to receive free email-alerts related to this article or journal.
Reprints and Subscriptions	To order reprints of this article or to subscribe to the journal, contact the AACR Publications Department at pubs@aacr.org.
Permissions	To request permission to re-use all or part of this article, use this link http://cancerres.aacrjournals.org/content/80/11/2273. Click on "Request Permissions" which will take you to the Copyright Clearance Center's (CCC) Rightslink site.